Electronic Supplementary Material (ESI) for New Journal of Chemistry.

Supplementary Materials

Construction of spin crossover-fluorescence bifunctional iron(II) complexes with modified bis(pyrazole)pyridine ligands

Guo-Hui Zhao[a], Shi-Hui Zhang[a], Cheng Yi[a], Tao Liu[a], Yin-Shan Meng*[a]

[a]*State Key Laboratory of Fine Chemicals, Dalian University of Technology, Dalian, 116024, P. R. China*

E-mail: mengys@dlut.edu.cn (Y. S. Meng)

Experimental section.

Materials

bpp-NH_2, bpp-I, bpp-CH_2Br, and bpp-$CH_2P(O)(OEt)_2$ were prepared according to literature methods[37-40]. The chemical reagents used are all analytical reagents sold on the market. If there is no special explanation in this paper, it is directly used.

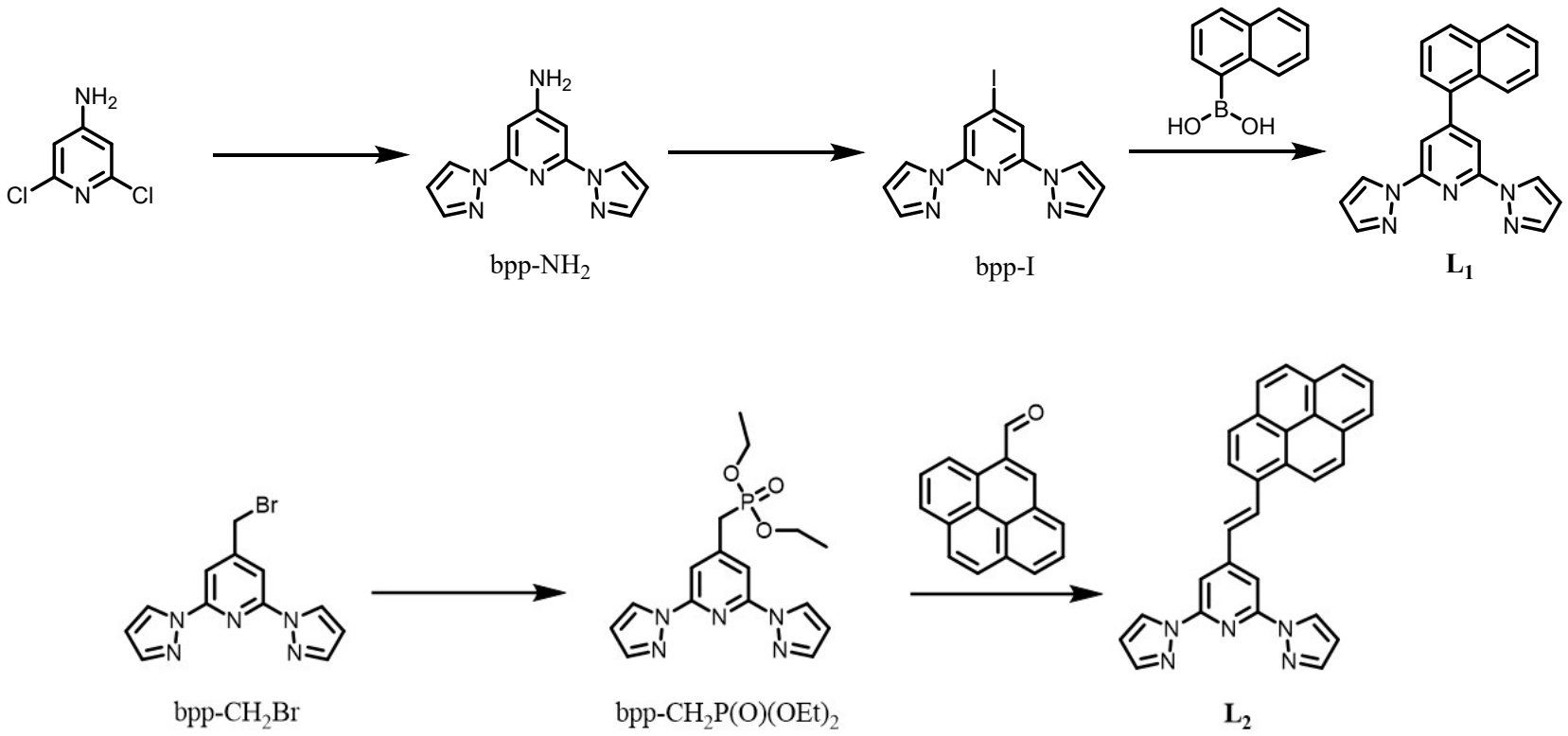

Scheme S1

Synthesis of ligand L_1

Under nitrogen condition, bpp-I (4.643 g, 13.8 mmol), 1-naphthoboric acid (2.37 g, 13.8 mmol) and pd(pph_3)$_4$ (1.581 g, 1.4 mmol) were added to 150 mL of 1, 4-dioxane and Na_2CO_3 solution (4.0 M, 50 mL) and stirred at 70 ℃ for reflux for 5 days. At the end of the reaction, the solvent was removed, followed by the extraction with 100 mL $CHCl_3$ for twice and washed with water for twice. The organic layer was then dried with anhydrous $MgSO_4$, and the solid was washed with methanol to remove soluble impurities. The crude product was purified by alumina column chromatography (ethyl acetate: n-hexane =1:4) to obtain the pure ligand **L_1**. ^{1}H NMR (500 MHz, Chloroform-d) δ 8.65–8.62 (m, 2H), 8.20 (s, 2H), 7.96–7.92 (m, 2H), 7.82 (s, 1H), 7.63–7.38 (m, 6H), 6.38–6.29 (m, 2H). MS (ESI-TOF): m/z 360.13 [M+Na]$^+$. Anal. Calcd for C21H15N5: C, 74.76; H, 4.48; N, 20.76. Found: C, 74.98; H, 4.31; N,20.41.

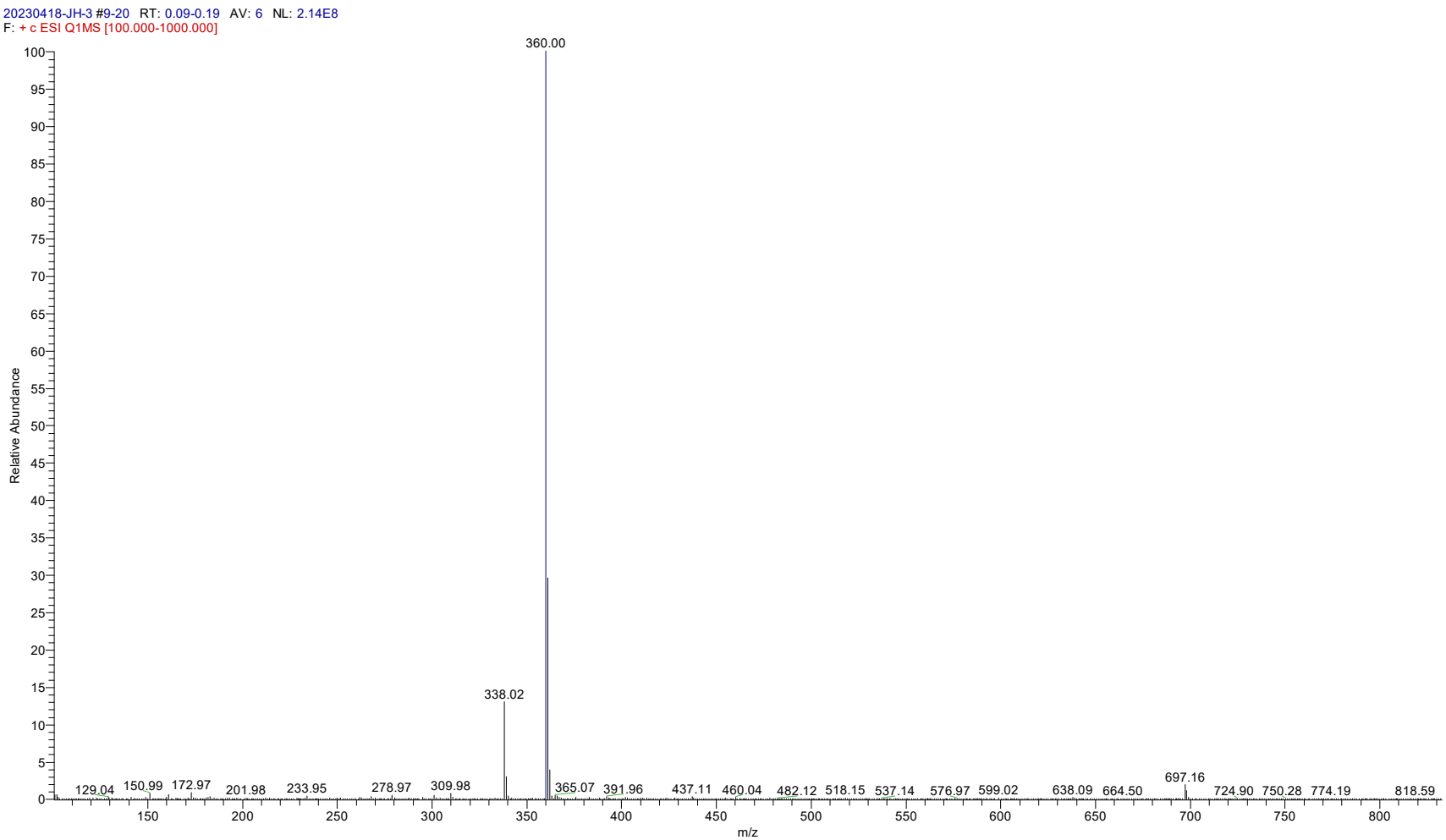

Fig. S1 The mass spectrometry of **L_1**.

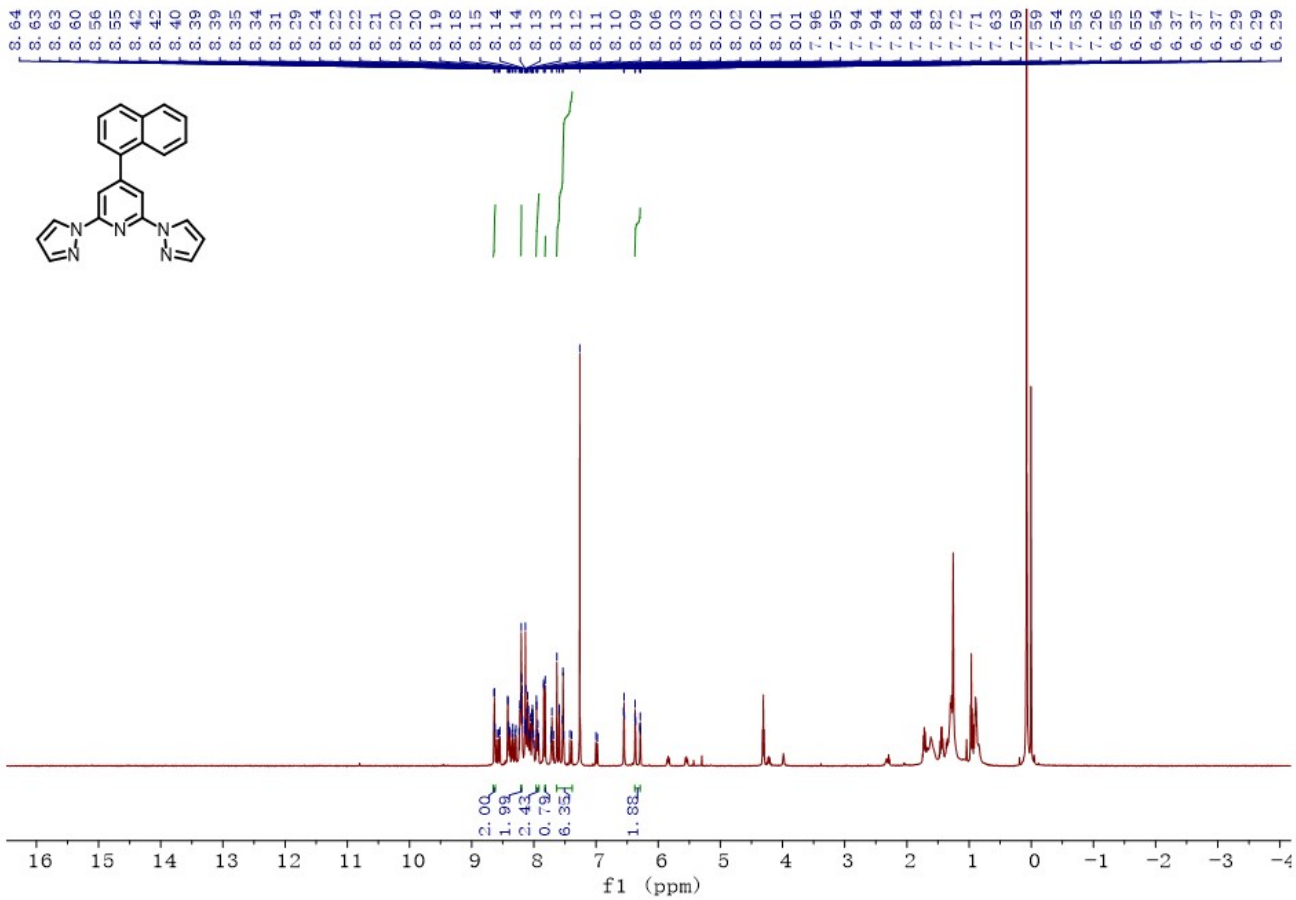

Fig. S2 ^{1}H NMR spectrum of $\mathbf{L_1}$ (500 MHz) in $CDCl_3$.

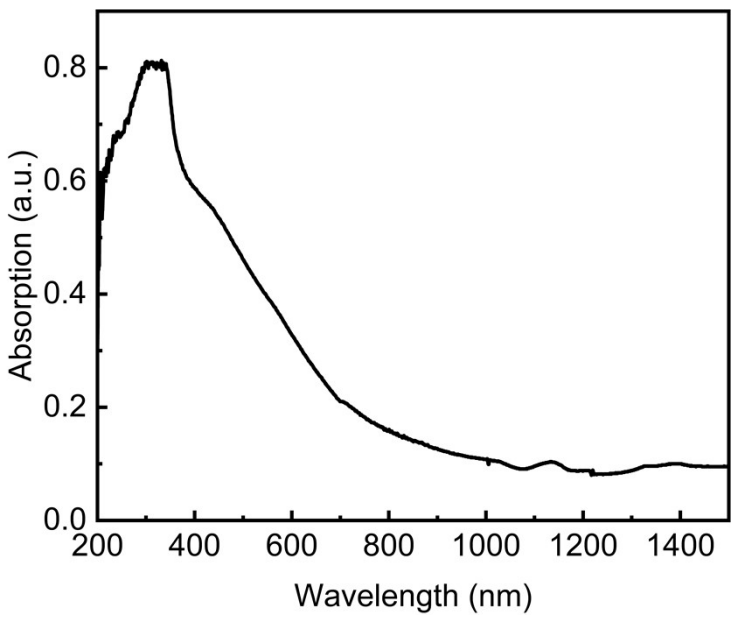

Fig. S3 UV–vis absorption spectroscopy of $\mathbf{L_1}$.

Synthesis of ligand L_2

bpp-$CH_2P(O)(OEt)_2$ (0.36 g, 1 mmol), 1-pyrene formaldehyde (0.17 g, 1 mmol) and 40 mL anhydrous THF solution were added to a 100 mL three-way flask and placed in an ice bath. Potassium tert-butanol (0.17 g, 1.5 mmol) was slowly added under nitrogen condition and stirred for 2 h. After the reaction, it was quenched with 15 mL water, extracted with CH_2Cl_2, washed with water for three times in the organic layer, and then washed with NaCl solution. The crude product was purified by column chromatography (ethyl acetate: n-hexane =5:95), and **L_2** obtained ^{1}H NMR (500 MHz, Chloroform-d) δ 8.67 (dd, J = 2.6, 0.7 Hz, 1H), 8.22–7.89 (m, 6H), 7.86–7.74 (m, 3H), 7.54–7.47 (m, 5H), 7.29 (dd, J = 8.3, 7.4 Hz, 1H), 6.82 (dd, J = 7.4, 1.1 Hz, 1H), 6.54 (dd, J = 2.7, 1.6 Hz, 2H). MS (ESI-TOF): m/z 460.16 $[M+Na]^+$. Anal. Calcd for C29H19N5: C, 79.61; H, 4.38; N, 16.01. Found: C, 79.93; H, 4.40; N,15.64.

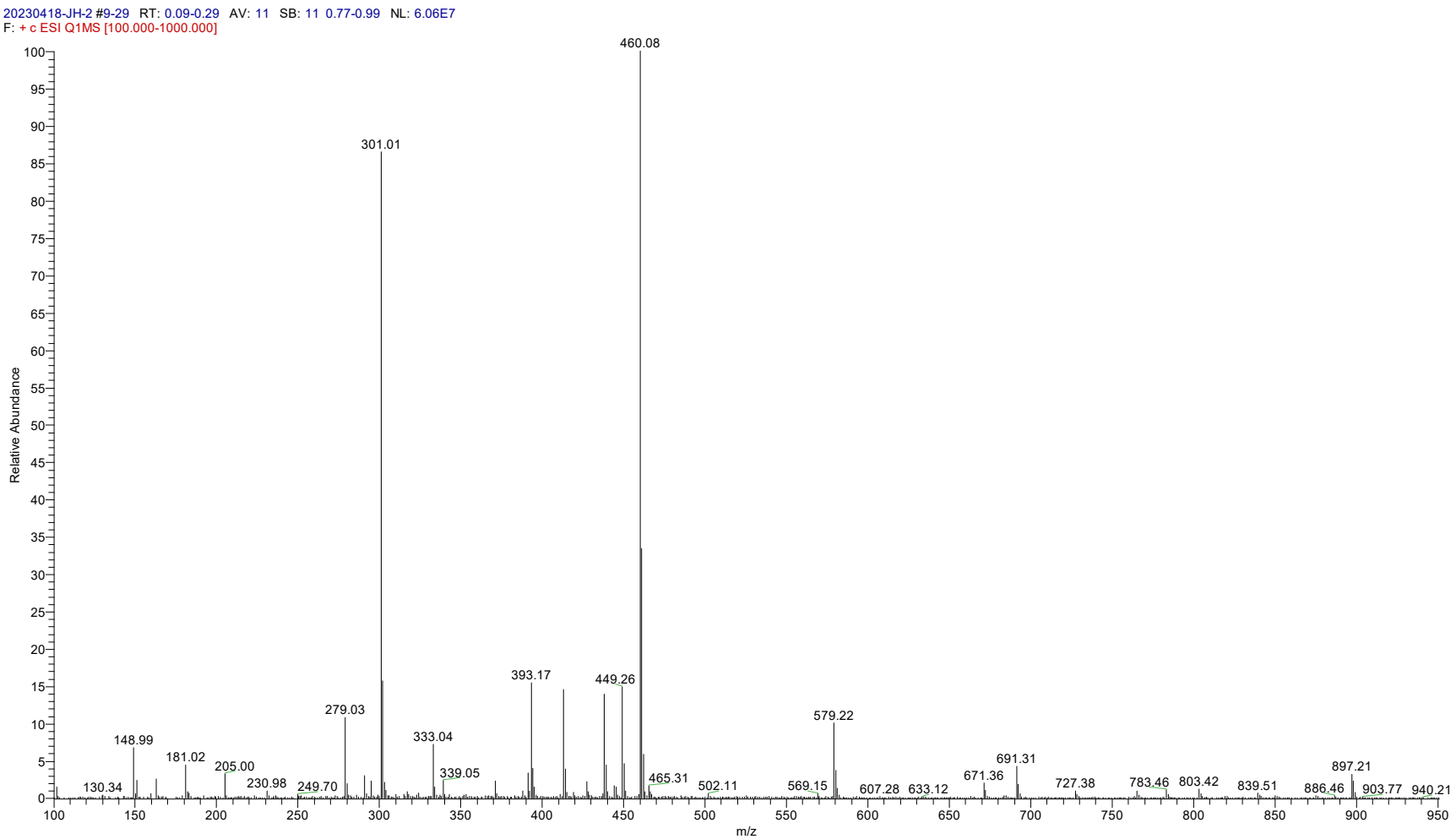

Fig. S4 The mass spectrometry of **L_2**.

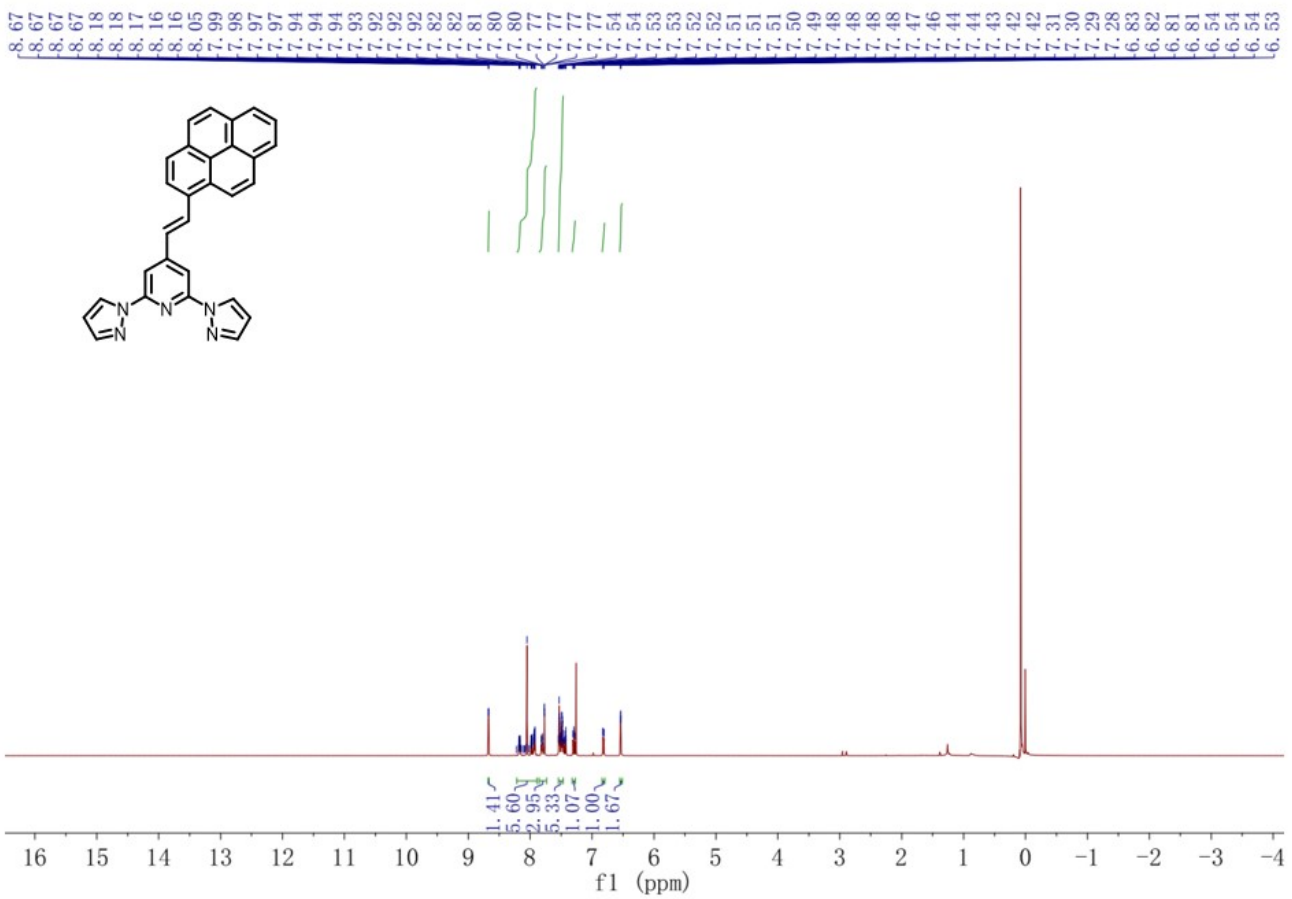

Fig. S5 ^{1}H NMR spectrum of $\mathbf{L_2}$ (500 MHz) in $CDCl_3$.

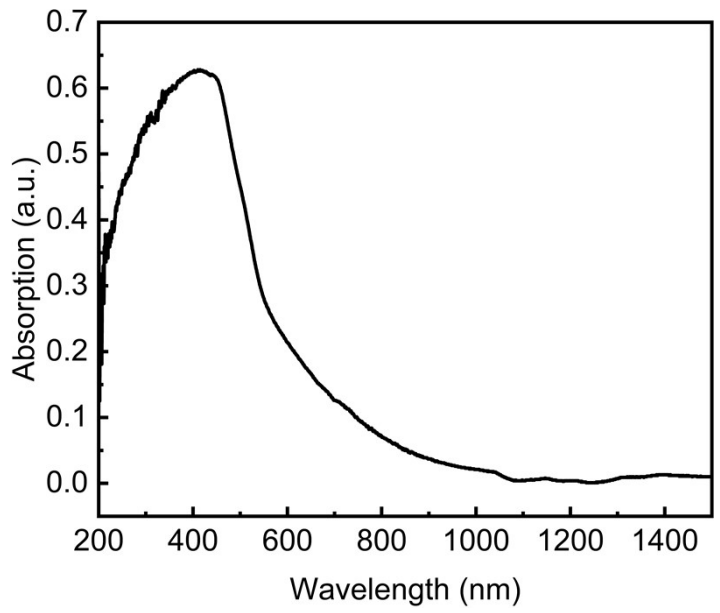

Fig. S6 UV–vis absorption spectroscopy of $\mathbf{L_2}$.

Table S1. Crystallographic data for **1** and **2** at different temperatures.

Compound	**1**	**1**	**2**
CCDC	2249925	2249928	2249929
T, K	120	400	120
formula	$C_{42}H_{30}Cl_2FeN_{10}O_8$	$C_{42}H_{30}Cl_2FeN_{10}O_8$	$C_{61}H_{46}Cl_8FeN_{10}O_9$
*F*w	929.51	929.51	1402.53
crystal system	Orthorhombic	Orthorhombic	Triclinic
Space group	*Pcca*	*Pcca*	$P\bar{1}$
a, Å	22.1519(13)	22.690(2)	13.5982(6)
b, Å	11.7439(7)	11.9056(11)	14.4074(7)
c, Å	14.6586(7)	14.9474(19)	17.2229(8)
α, °	90	90	96.619(2)
β, °	90	90	102.0490(10)
γ, °	90	90	113.550(2)
V, Å^3	3813.4(4)	4037.8(7)	2949.8(2)
Z	8	8	2
ρ_{calc}g/cm^3	1.619	1.529	1.579
F (000)	1904.0	1904.0	1432.0
Reflections collected	28492	18741	75707
Unique reflections (R_{int})	5451	4127	13508
Goodness–of–fit on F^2	1.021	1.083	1.048
R_1 [I≥2σ(I)]a	0.0543	0.1179	0.0872
wR_2[I≥2σ(I)]b	0.1207	0.1915	0.2550

$R_1 = \Sigma\,(|F_o|-|F_c|) / \Sigma\,|F_o|$; $wR_2 = [\Sigma\, w\,(|F_o|-|F_c|)^2 / \Sigma\, w\, F_o^2]^{1/2}$

Table S2. Selected Bond lengths (Å) for **1** and **2** at different temperatures.

1			**2**	
	120 K	400 K		120 K
No	Length(Å)	Length(Å)	No	Length(Å)
Fe1–N1	1.8964(19)	2.054(6)	Fe1–N1	1.888(3)
Fe1–N1	1.8964(19)	2.054(6)	Fe1–N2	1.976(3)
Fe1–N2	1.964(2)	2.110(7)	Fe1–N3	1.981(4)
Fe1–N2	1.964(2)	2.110(7)	Fe1–N4	1.890(3)
Fe1–N3	1.966(2)	2.112(7)	Fe1–N5	1.970(4)
Fe1–N3	1.966(2)	2.112(7)	Fe1–N6	1.963(4)
$Fe1–N_{avg}$	1.942	2.092	$Fe1–N_{avg}$	1.944

Table S3. Selected Bond Angles (º) for **1** at different temperatures.

Compound	**1**	
Temperature(K)	120	400
N1–Fe1–N1	178.47(13)	176.6(4)
N1–Fe1–N3	98.95(9)	75.0(3)
N1–Fe1–N3	79.96(9)	107.4(3)
N1–Fe1–N3	79.96(9)	75.0(3)
N1–Fe1–N3	98.95(9)	107.4(3)
N1–Fe1–N2	80.09(9)	102.4(3)
N1–Fe1–N2	100.98(9)	75.2(3)
N1–Fe1–N2	80.09(9)	75.2(3)
N1–Fe1–N2	100.98(9)	102.4(3)
N3–Fe1–N3	90.57(13)	93.9(4)
N2–Fe1–N3	91.92(9)	150.2(3)
N2–Fe1–N3	160.04(8)	94.7(3)
N2–Fe1–N3	91.92(9)	94.7(3)
N2–Fe1–N3	160.04(8)	150.2(3)
N2–Fe1–N2	92.47(13)	91.9(4)
Σ_{Fe}	86.64	134.4
$CShM_{Fe}$	2.061	4.522

Σ_{Fe} : the sum of | 90-α |for the 12 *cis*-N-Fe-N angles around the iron atom. $CShM_{Fe}$: the continuous shape measurement relative to ideal octahedron of the Fe center.

Table S4. Selected Bond Angles (º) for **2** at 120 K.

Compound	**2**
Temperature(K)	120
N2–Fe1–N3	160.00(13)
N4–Fe1–N2	99.03(13)
N4–Fe1–N5	80.13(14)
N4–Fe1–N6	80.35(14)
N4–Fe1–N3	100.96(14)
N1–Fe1–N2	80.12(13)
N1–Fe1–N4	175.44(15)
N1–Fe1–N5	104.33(14)
N1–Fe1–N6	95.21(14)
N1–Fe1–N3	79.97(14)
N5–Fe1–N2	90.15(14)
N5–Fe1–N3	92.92(16)
N6–Fe1–N2	93.69(14)
N6–Fe1–N5	160.46(13)
N6–Fe1–N3	89.98(16)
Σ_{Fe}	85.74
$CShM_{Fe}$	2.132

Σ_{Fe} : the sum of | 90-α |for the 12 *cis*-N-Fe-N angles around the iron atom. $CShM_{Fe}$: the continuous shape measurement relative to the ideal octahedron of the Fe center.

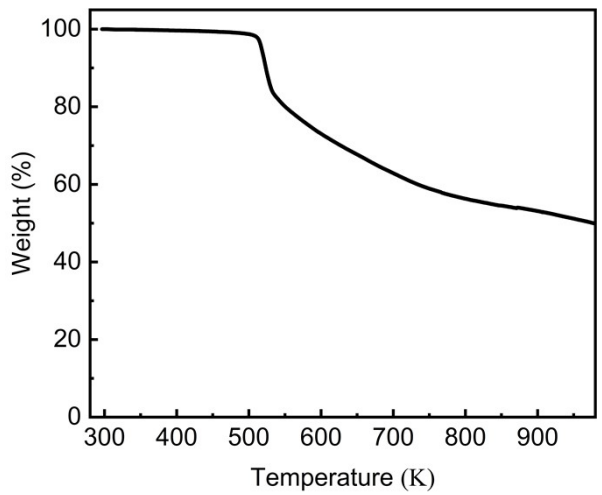

Fig. S7 TGA curve for complex **1** in N_2 atmosphere with a heating rate of 10 $K \cdot min^{-1}$.

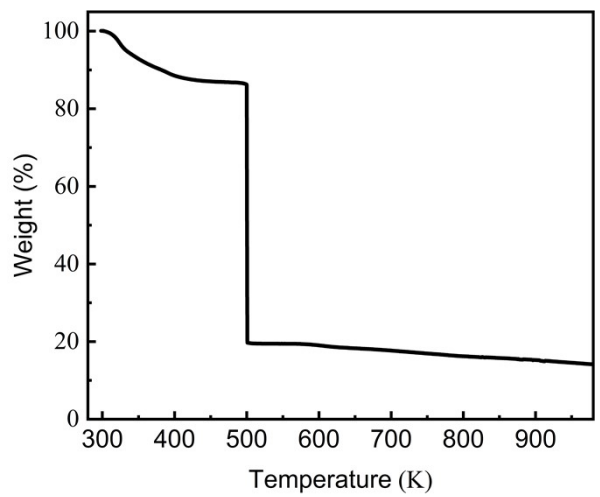

Fig. S8 TGA curve for complex **2** in N_2 atmosphere with a heating rate of 10 $K \cdot min^{-1}$.

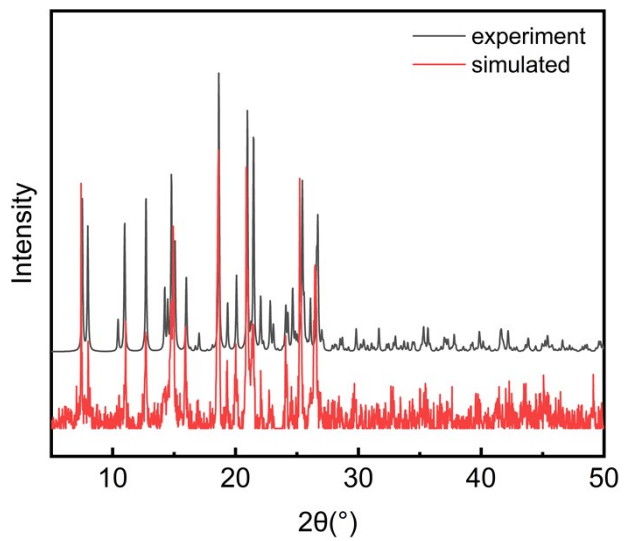

Fig. S9 The PXRD pattern of complex **1** and the simulated one based on the single-crystal structure.

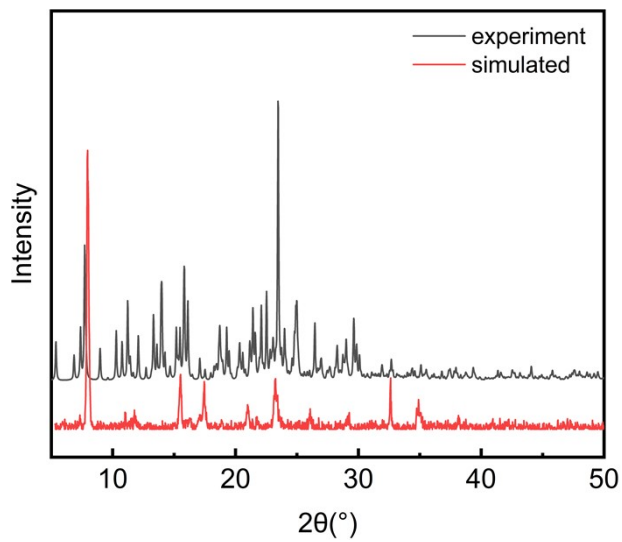

Fig. S10 The PXRD pattern of complex **2** and the simulated one based on the single-crystal structure.

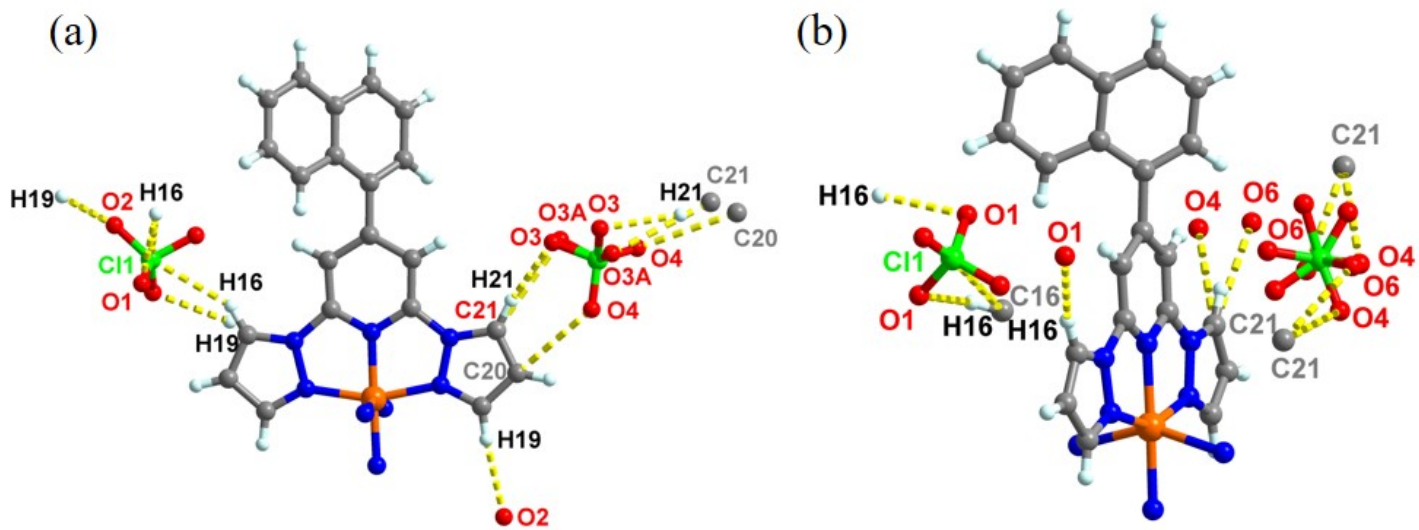

Fig. S11 The intermolecular short contact interactions (yellow dashed lines) for **1** at 120K (a) and 400 K (b).

Table S5. Short contact interactions for **1** at 120 and 400 K.

1			
120 K		400 K	
C16 – H16···Cl 1	3.574(25)		
C16 – H16···O1	3.260(32)	C16 – H16···Cl 1 [x,-y+1,z-1/2]	3.670(98)
C16 – H16···O1 [-x+3/2,-y+1,z]	3.368(32)	C16 – H16···O1 [-x+3/2,y,z-1/2]	3.252(121)
C18 – H18···O4 [-x+3/2,y,z-1/2]	3.562(35)	C18 – H18···O5 [x+1/2,-y,-z+1/2]	3.510(186)
C19 – H19···O2 [-x+3/2,y+1,z+1/2]	3.400(31)		
C20 – H20···O4	3.138(36)		
C21 – H21···O3	3.238(56)	C21 – H21···O4 [x,-y,z+1/2]	3.167(175)
C21 – H21···O3A	3.181(54)	C21 – H21···O6 [-x+1,-y,-z+1]	3.175(184)

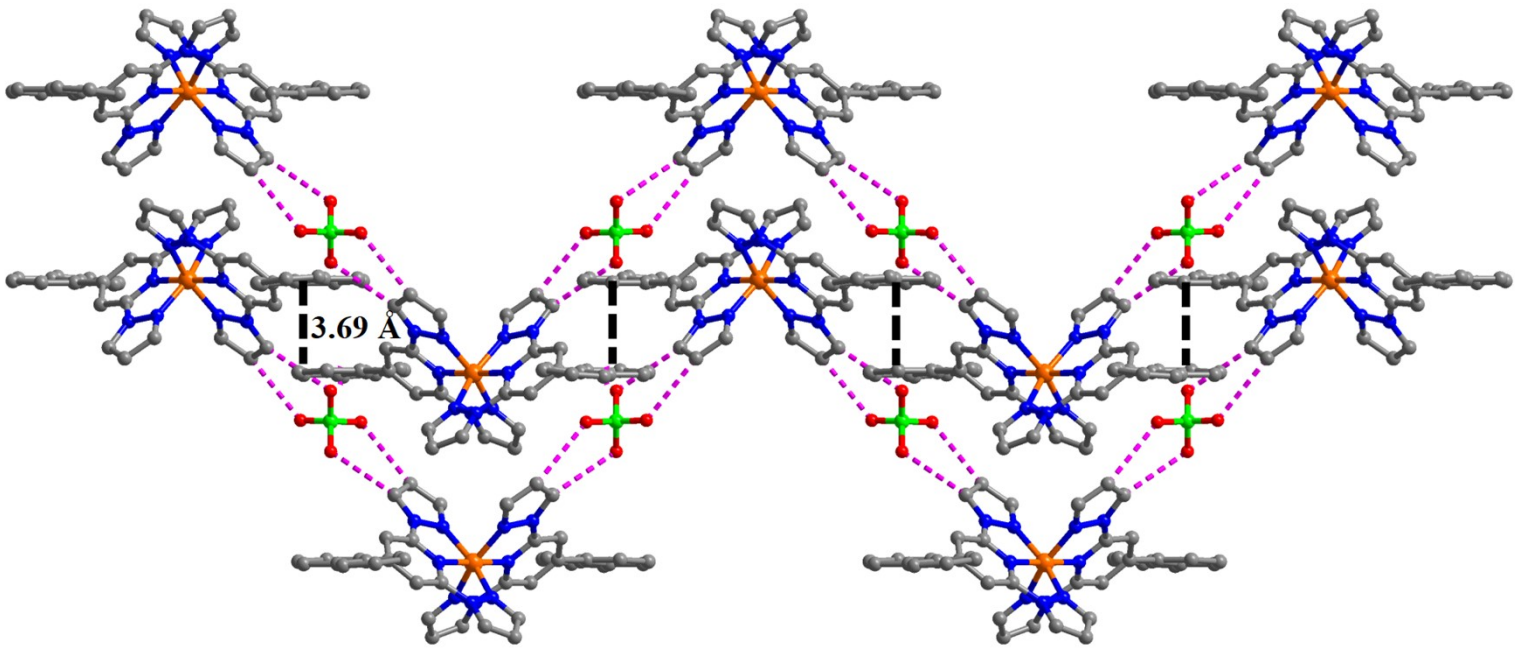

Fig. S12 The molecular packing of **1** at 400 K. The black dashed lines represent π···π interactions, and the pink dashed lines represent C–H···O hydrogen bonds.

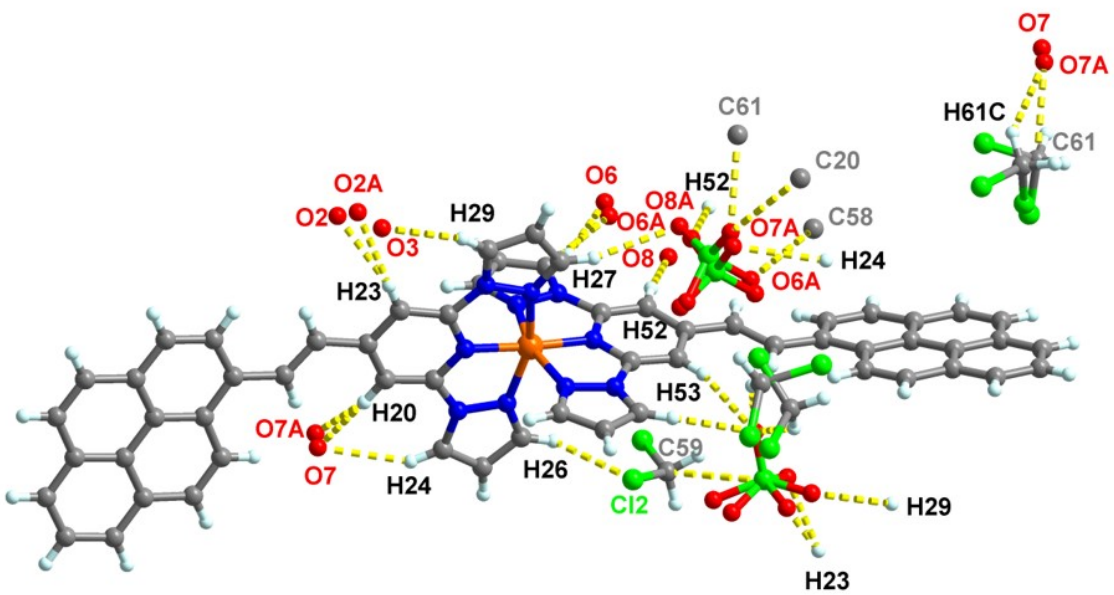

Fig. S13 The intermolecular short contact interactions (yellow dashed lines) for **2** at 120K.

Table S6. Short contact interactions for **2** at 120 K.

2			
C20 – H20···O7^a [x-1,y,z]	3.302(5)	C52 – H52···O8^a [-x+1,-y+1,-z+1]	3.415(6)
C20 – H20···O7A^b [x-1,y,z]	3.20(3)	C52 – H52···O8A^b [-x+1,-y+1,-z+1]	3.52(3)
C23 – H23···O2^a [x,y+1,z]	3.271(8)	C53 – H53···O4	3.409(3)
C23 – H23···O2A^b [x,y+1,z]	3.222(14)	C58 – H58···O6^a [-x+1,-y+1,-z+1]	3.328(6)
C24 – H24···O7^a [x-1,y,z]	3.455(6)	C58 – H58···O6A^b [-x+1,-y+1,-z+1]	3.11(3)
C26 – H26···Cl 1	3.803(6)	C60^a - H60B^a···O4	3.305()
C26 – H26···Cl 2	3.404(4)	C60A^b - H60D^b···O4	3.143(6)
C27 – H27···O8A^b	3.53(2)	C61^a - H61A^a···O7^a [-x+2,-y+1,-z+1]	3.245(8)
C29 – H29···O3^a [x,y+1,z]	3.473(8)	C61A^b - H61C^bO7A^b [-x+2,-y+1,-z+1]	3.37(4)
C49 – H49A···O4	3.325(3)		

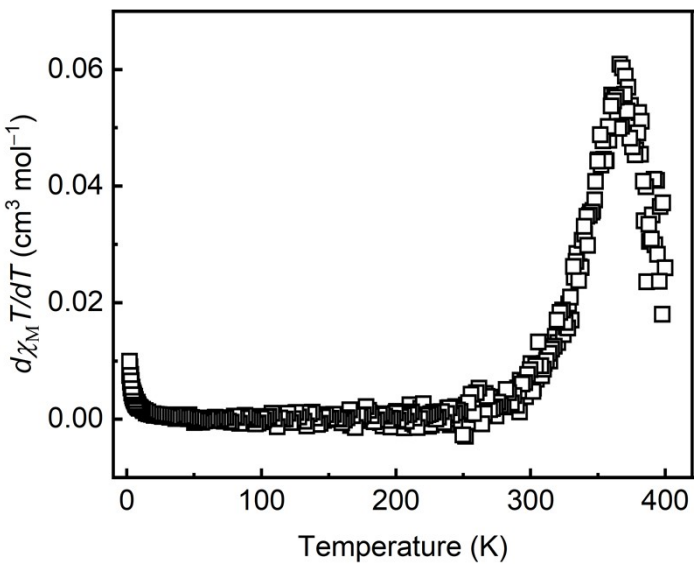

Fig. S14. d($\chi_M T$)/dT versus T for complex **1**.

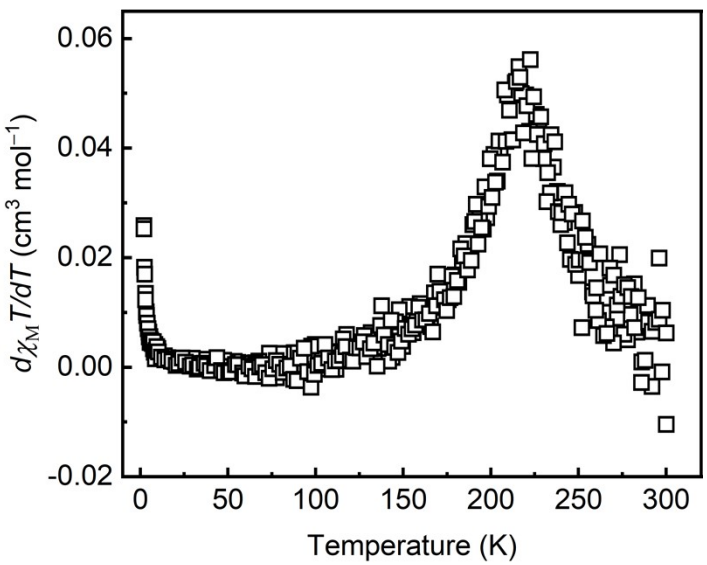

Fig. S15. d($\chi_M T$)/dT versus T for complex **2**.

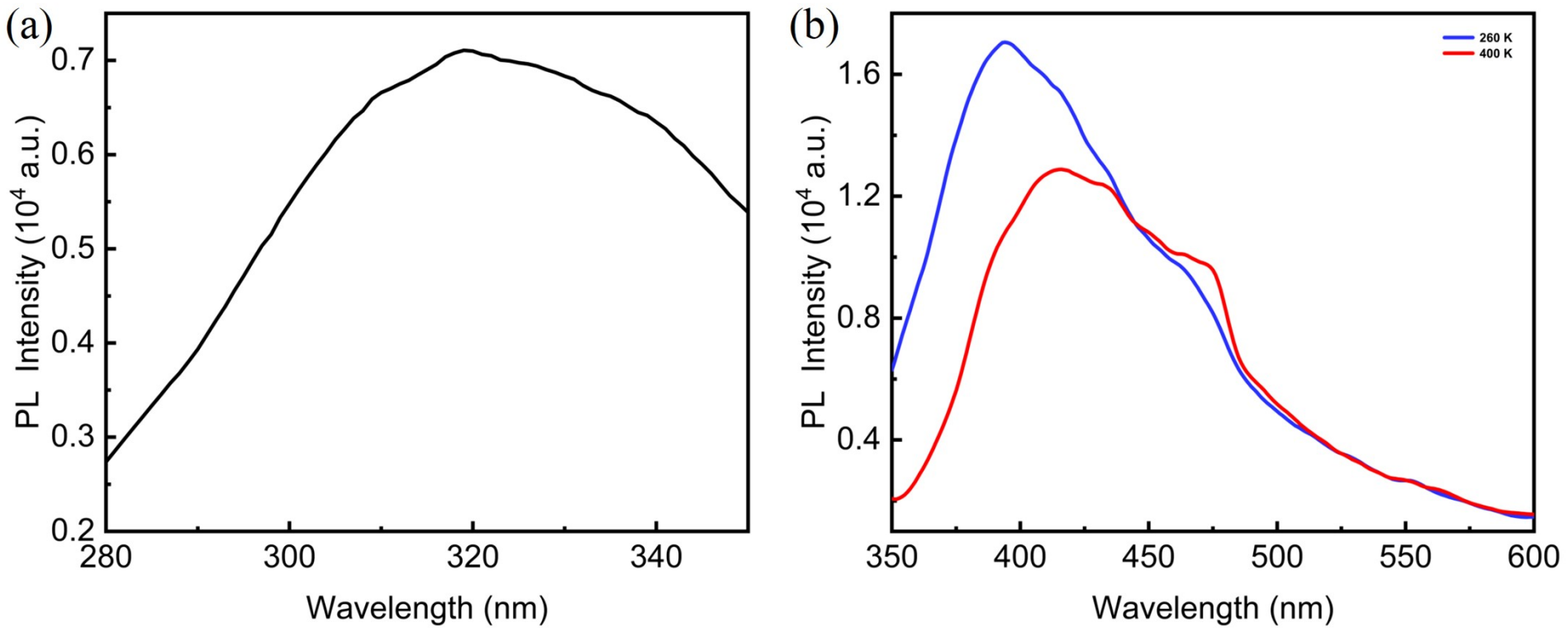

Fig. S16 (a) Luminescence excitation spectrum for the complex **1** in the solid state at 260 K (λ_{ex} = 320 nm). (b) Luminescence emission spectra for the complex **1** in the solid state at 260 K (blue) and 400 K (red).

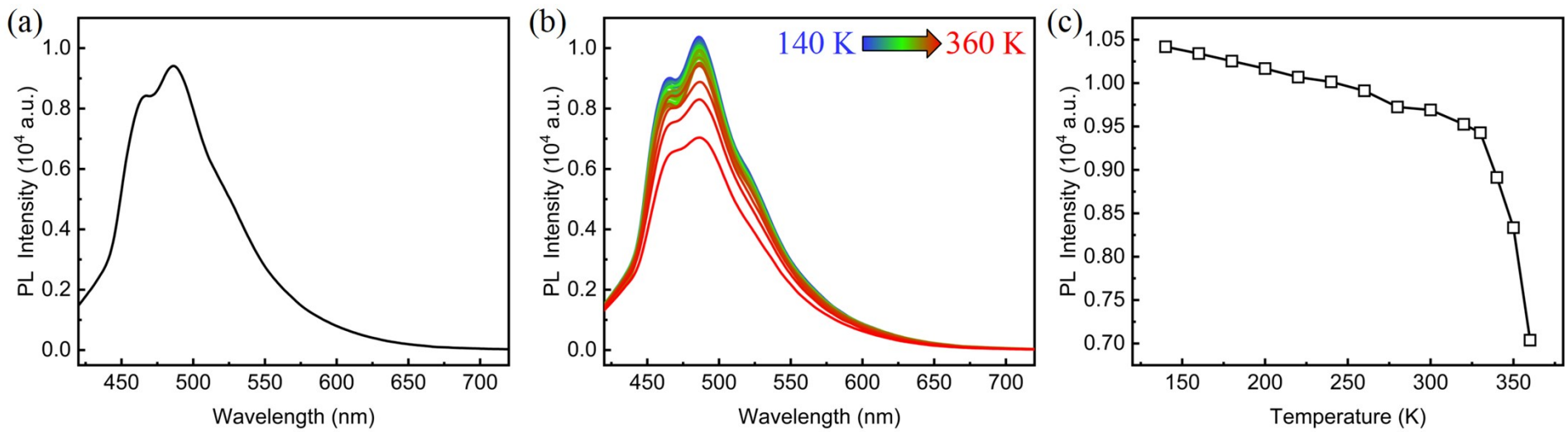

Fig. S17 (a) Luminescence emission spectra for the ligand $\mathbf{L_1}$ at 300 K (λ_{ex} = 387 nm). (b) Temperature-dependent luminescence emission spectra for ligand $\mathbf{L_1}$ (λ_{em} = 485 nm). (c) Maximum of luminescence emission intensity as a function of temperature for ligand $\mathbf{L_1}$.

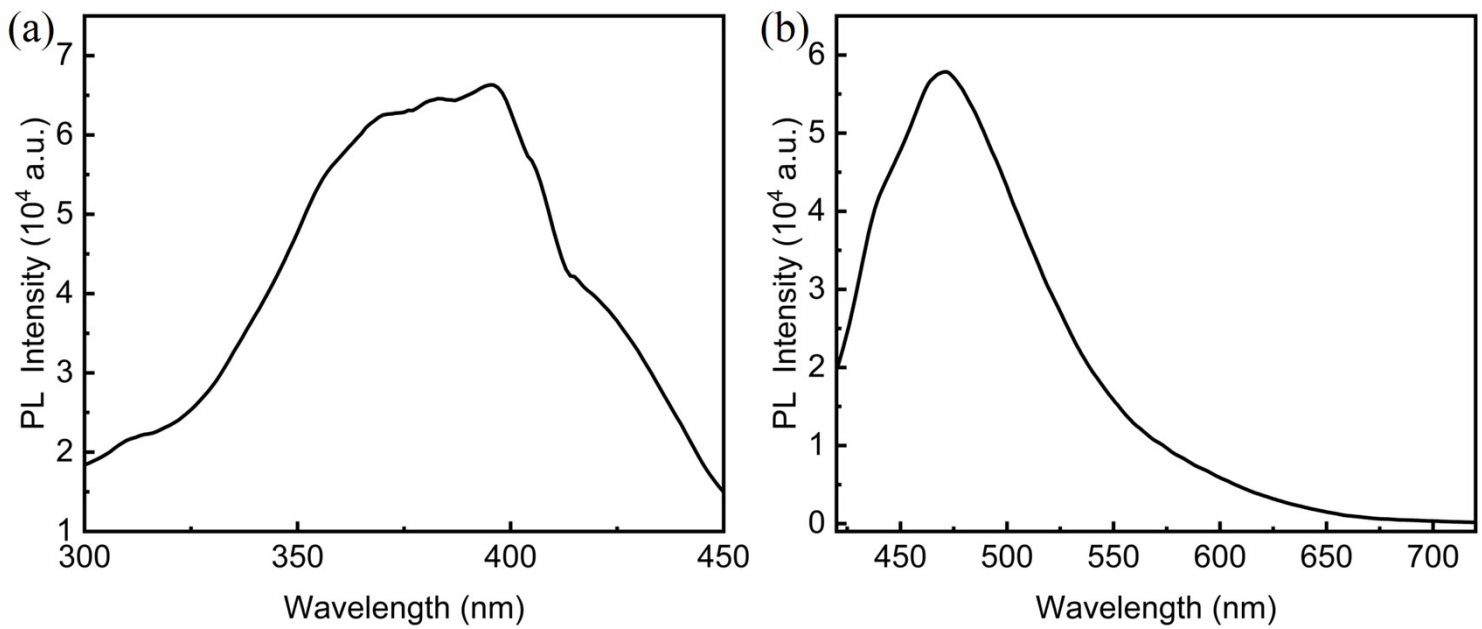

Fig. S18 (a) Luminescence excitation spectrum for the complex **2** in the solid state at 300 K (λ_{ex} = 395 nm). (b) Luminescence emission spectra for the complex **2** in the solid state at 300 K (λ_{ex} = 475 nm).

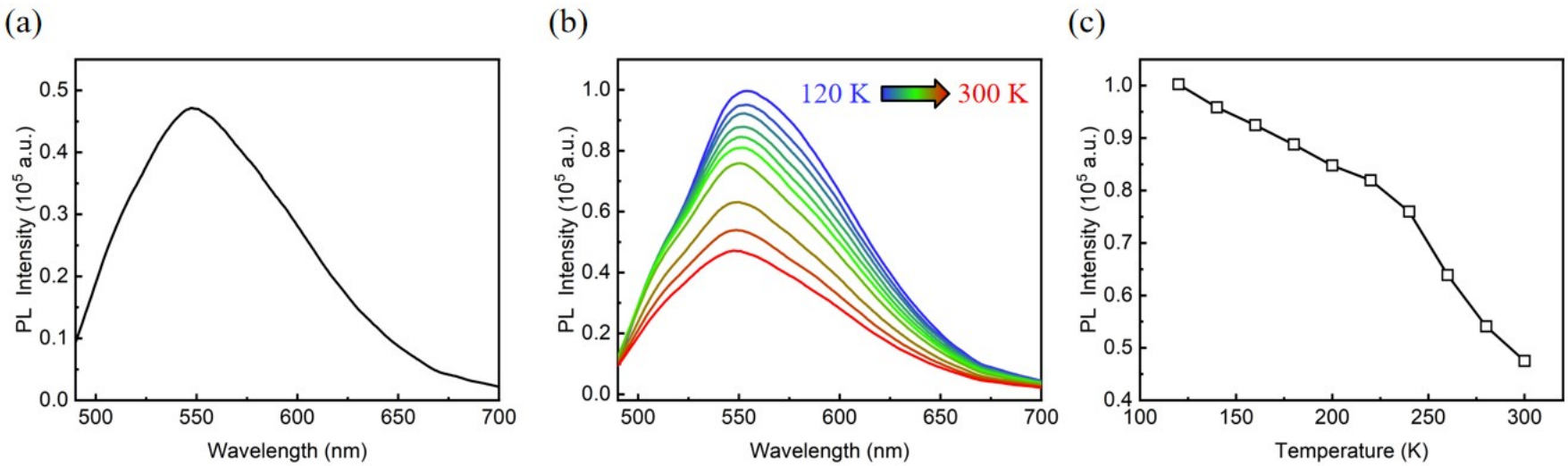

Fig. S19 (a) Luminescence emission spectra for the ligand $\mathbf{L_2}$ at 300 K (λ_{ex} = 467 nm). (b) Temperature-dependent luminescence emission spectra for ligand $\mathbf{L_2}$ (λ_{em} = 550 nm). (c) Maximum of luminescence emission intensity as a function of temperature for ligand $\mathbf{L_2}$.

Evans' method

Solution magnetic susceptibility data were measured according to the literature's procedure in the temperature range from 268 to 373 K by ^{1}H NMR spectroscopy on a Bruker 400 MHz spectrometer using Evans' method. At each temperature point we waited for 15 minutes before measurement. Pure sample of 1 (4.8 mg) was dissolved in 0.7 mL of DMF-d_7. Pure DMF-d_7 was placed in a capillary insert, and the paramagnetic solution was placed in the outer tube. The calculation equation is as follows:

$$\chi_M T = \left(\frac{3\Delta f}{4\pi m f} M + \chi_M^{dia}\right) \times T$$

Where m is the concentration of the paramagnetic solution in g mL^{-1}, f is the spectrometer frequency in Hz, Δf is the shift of the DMF-d_7 peak in the paramagnetic solution compared to pure DMF-d_7 in Hz. $\chi_M^{dia} = M \times 10^{-6}$ cm^3 mol^{-1} (M is the molecular weight).

Table S7. The calculated $\chi_M T$ values for **1** at multiple temperatures according to the Evans' method.

T (K)	268	273	293	313	333	353	373
$f1$ (Hz)	1290.64	1285.26	1265.98	1251.82	1238.01	1227.39	1289.02
$f2$ (Hz)	1100.05	1100.05	1100.05	1100.51	1100.05	1100.05	1100.05
Δf (Hz)	190.59	185.21	165.93	151.31	137.96	127.34	188.97
$\chi_M T$ (cm^3 mol^{-1} K)	3.48	3.41	3.44	3.42	3.38	3.37	3.45

(a)

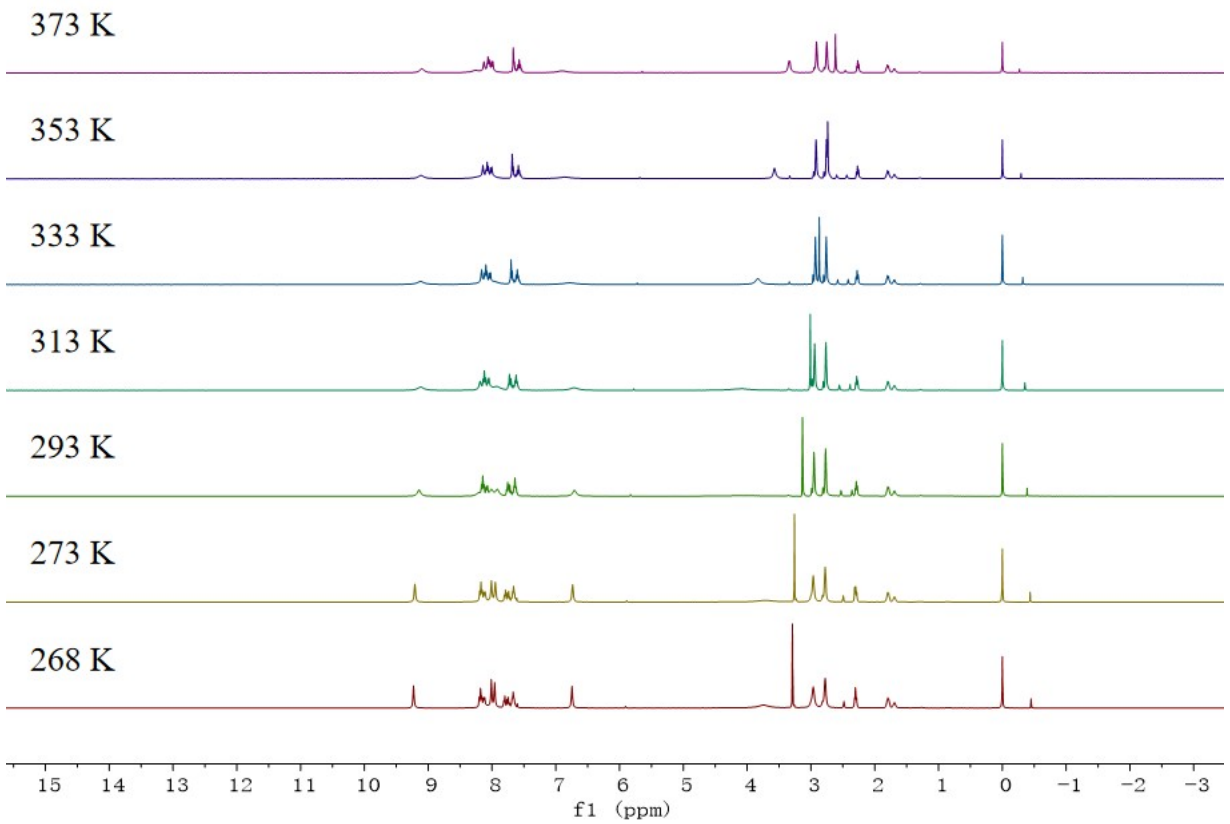
373 K
353 K
333 K
313 K
293 K
273 K
268 K
15 14 13 12 11 10 9 8 7 6 5 4 3 2 1 0 −1 −2 −3
f1 (ppm)

(b)

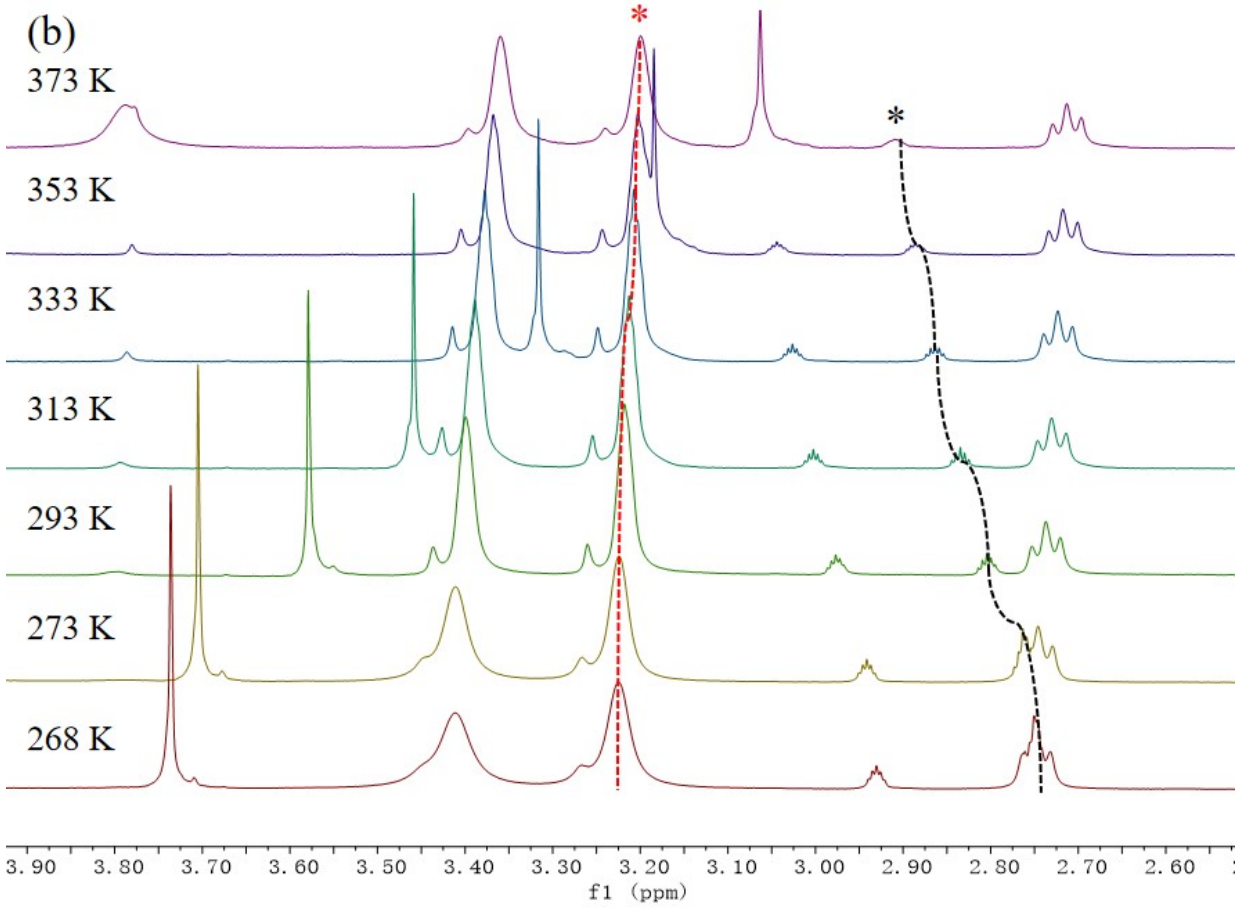
373 K
353 K
333 K
313 K
293 K
273 K
268 K
*
*
3.90 3.80 3.70 3.60 3.50 3.40 3.30 3.20 3.10 3.00 2.90 2.80 2.70 2.60
f1 (ppm)

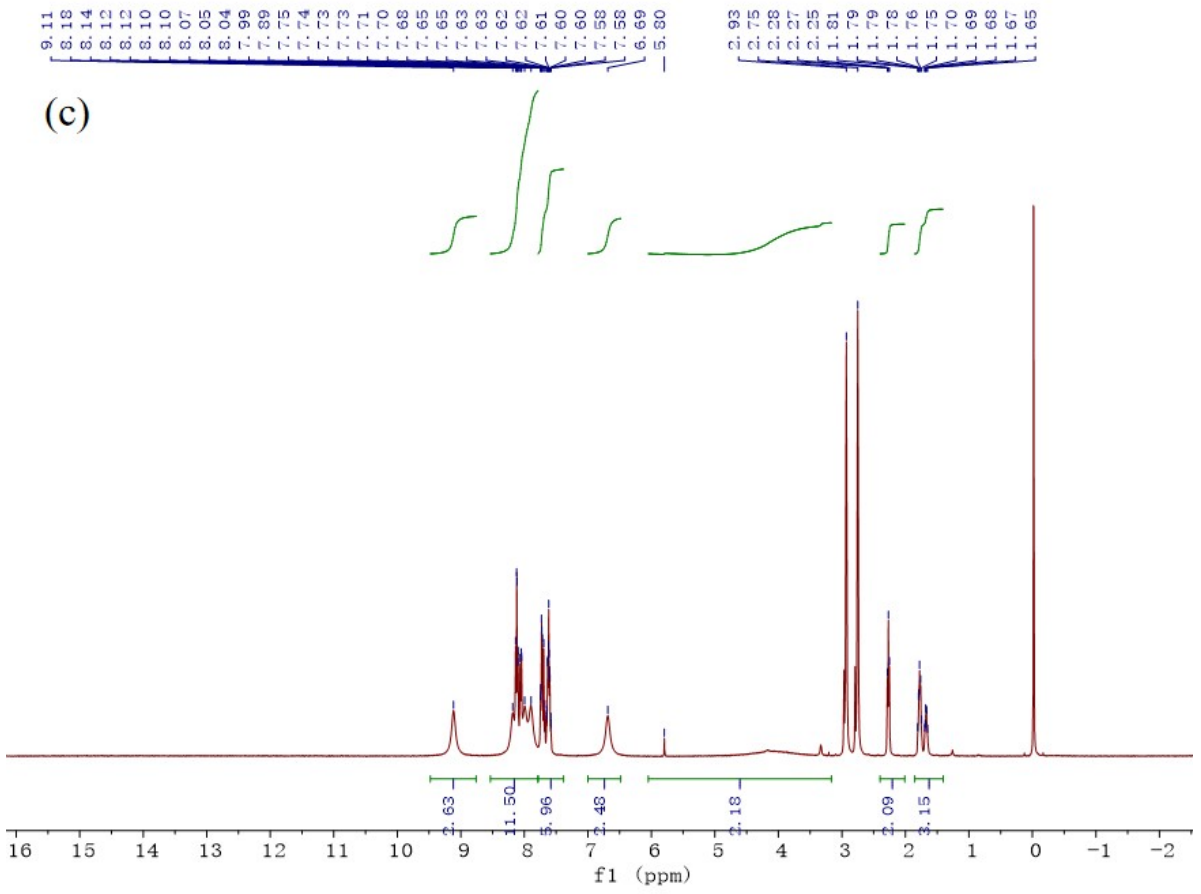

Fig. S20. (a) Stacked spectra, obtained by the Evans ^{1}H NMR method, from 373 to 268 K for **1** (5.0×10^{-3} mol L^{-1}) in DMF-d_7 (400 MHz). (b) The enlarged region of solvent residual peaks (* and * represent the solvent residual signals in solution and in the inner tube, respectively). (c) ^{1}H NMR spectrum of complex **1** in DMF-d_7 at room temperature.

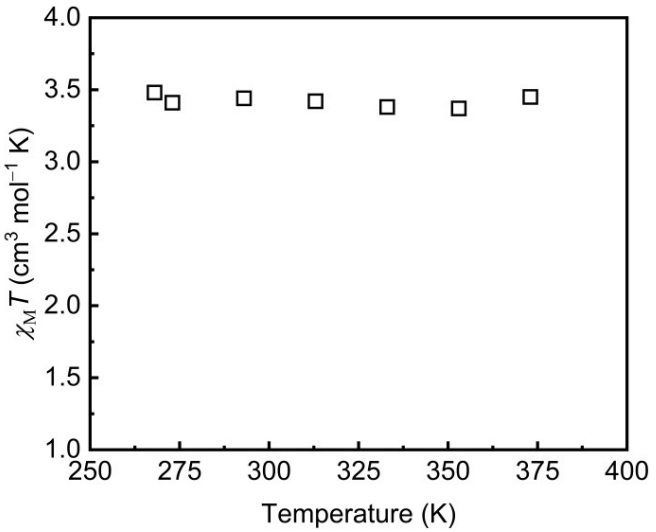

Fig. S21 $\chi_M T$ vs T of compound **1** in DMF-d_7 solution state Evans method studies (400 MHz).

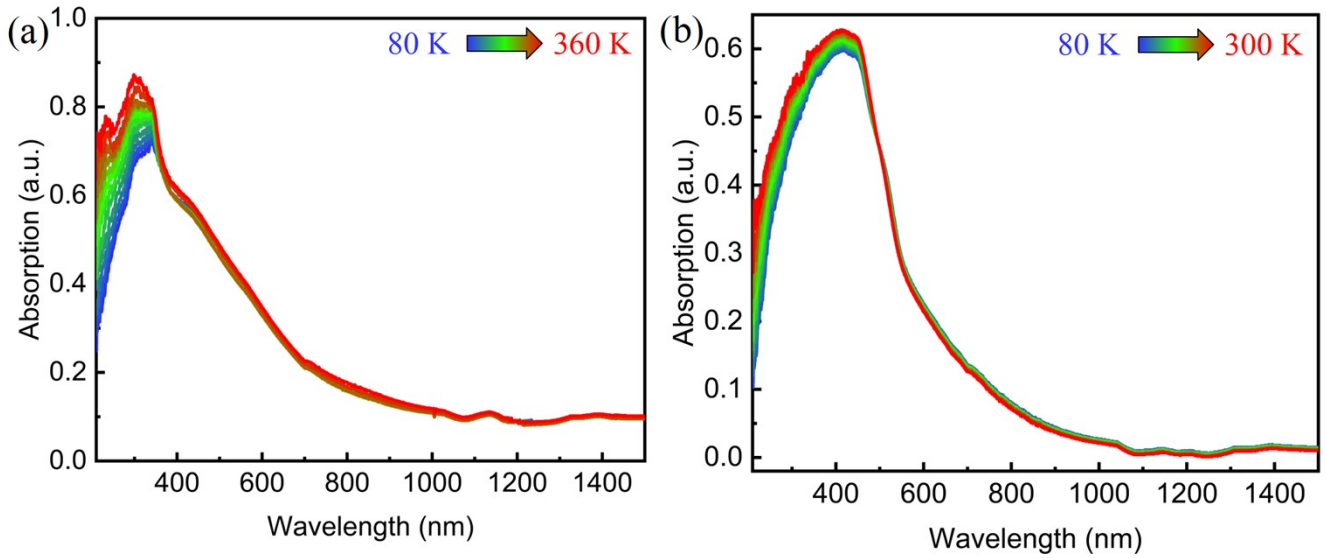

Fig. S22 Temperature-dependent UV–vis absorption spectroscopy of $\mathbf{L_1}$ (a) and $\mathbf{L_2}$ (b) in the solid state.

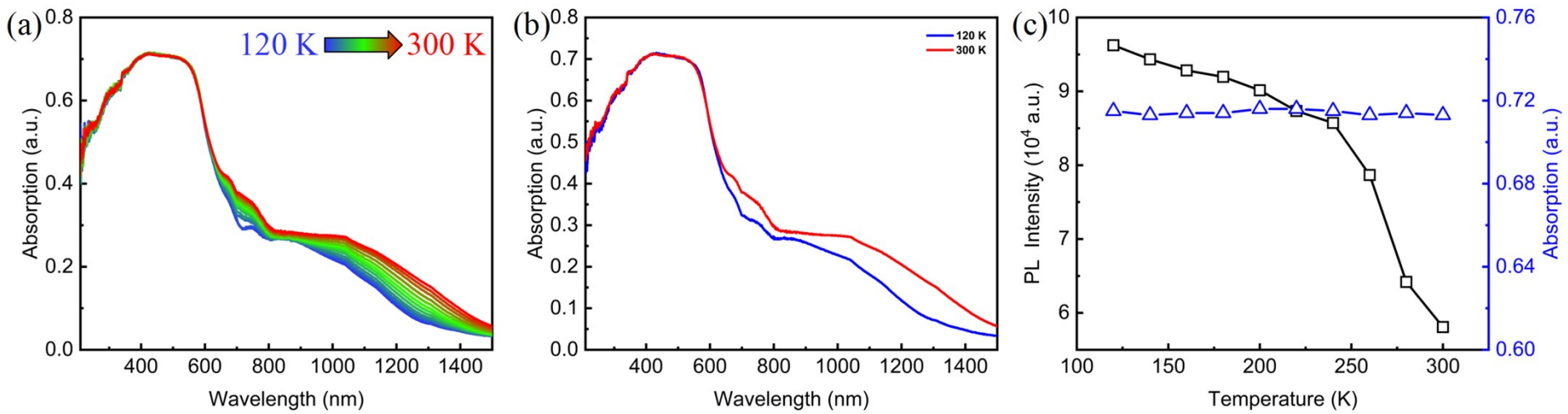

Fig. S23 (a) Temperature-dependent UV–vis absorption spectroscopy of **2** in the solid state. (b) Temperature-dependent UV–vis absorption spectroscopy of **2** in the solid state at 120 K (blue line) and 300 K (red line). (c) The PL intensity of the maximum emission (λ_{em} = 475 nm) (black squares) and absorption intensity centering at 500 nm (blue triangles) profiles as a function of temperature for **2**.

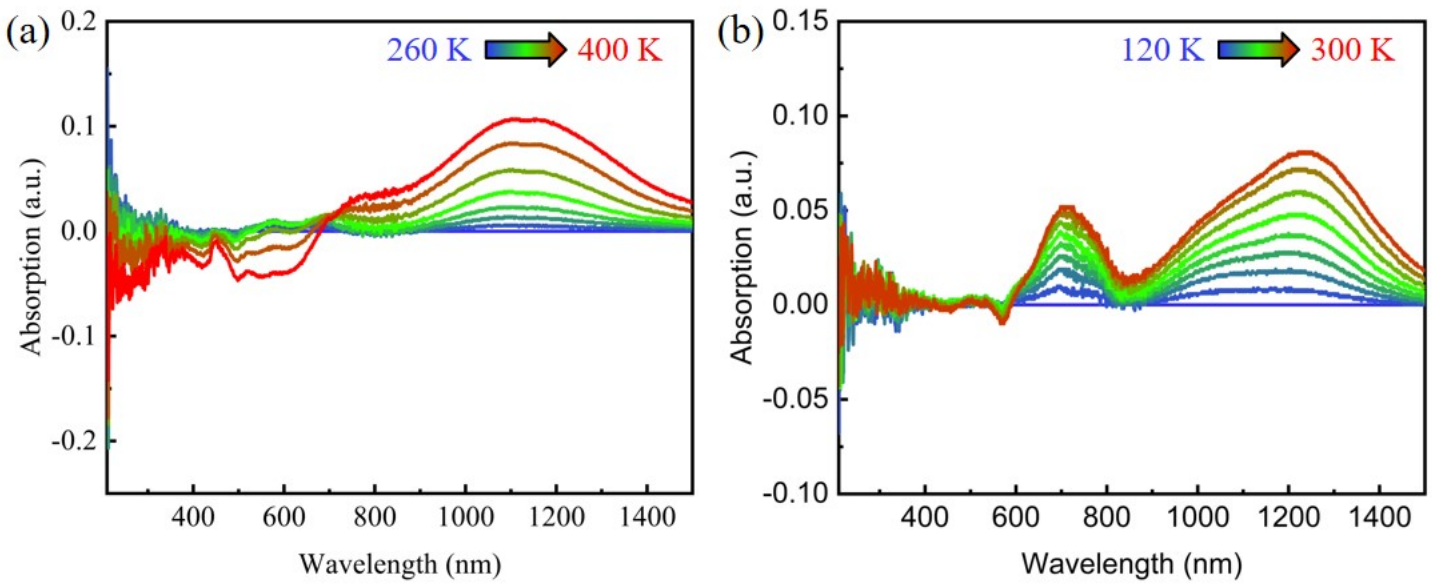

Fig. S24 The margin calculation between the UV-vis absorption spectrum and the low temperature spectrum of the complex **1** (a) and **2** (b).

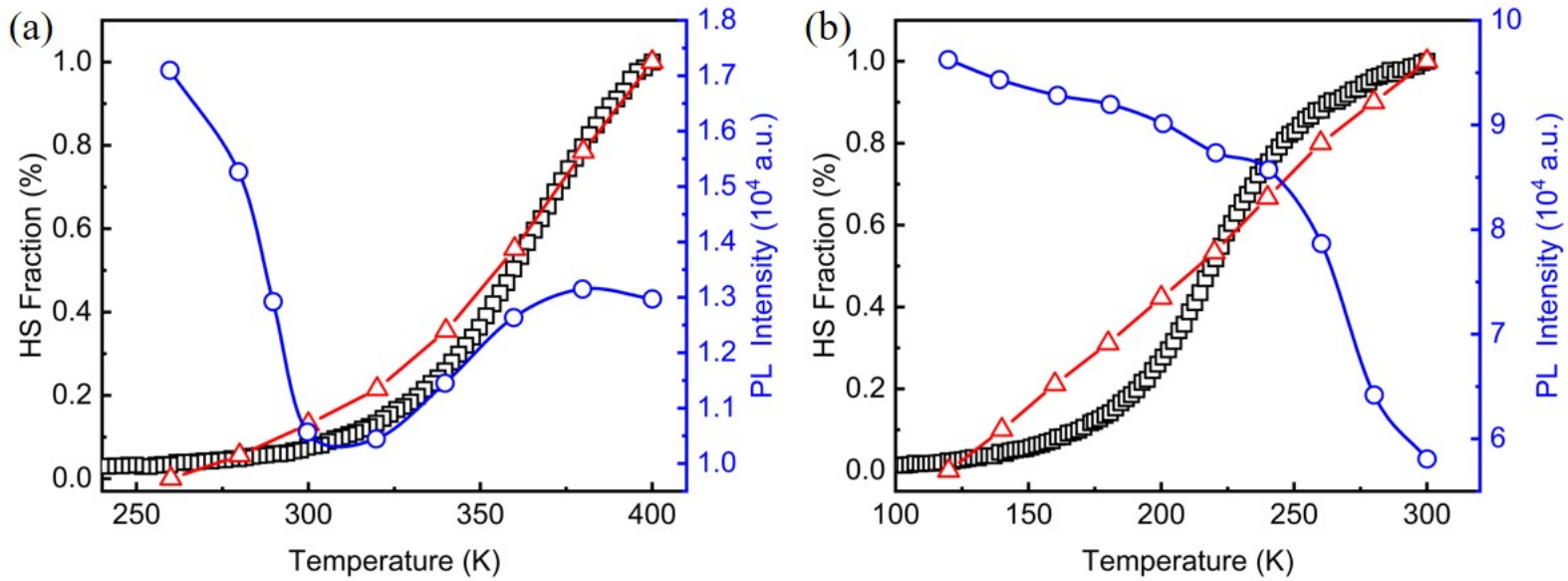

Fig. S25 Diagram of HS fraction (black square) and maximum luminescent emission intensity (blue circle) of Fe^{II} ions in **1** and **2** as a function of temperature, and reconstruction of HS fraction by UV-vis absorption spectra measurements (red triangle).

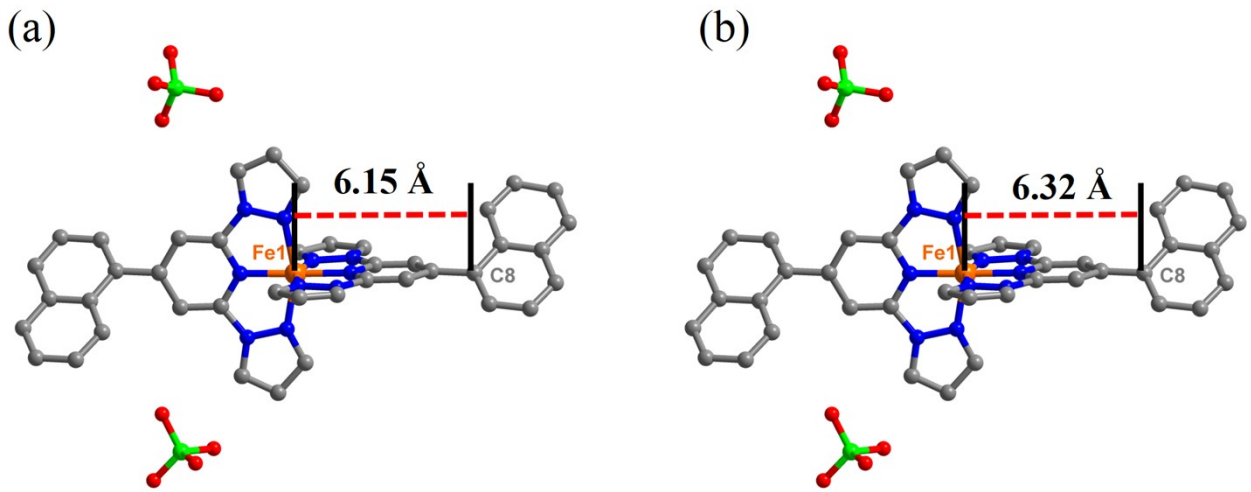

Fig. S26 Complex **1** at different temperatures, the distance between the Fe^{II} center and the modified group (a) 120 K; (b) 400 K. All H atoms and solvent molecules are omitted for clarity. (Atomic colour scheme: Fe, orange; C, gray; O, red; N, blue; Cl, bright green).

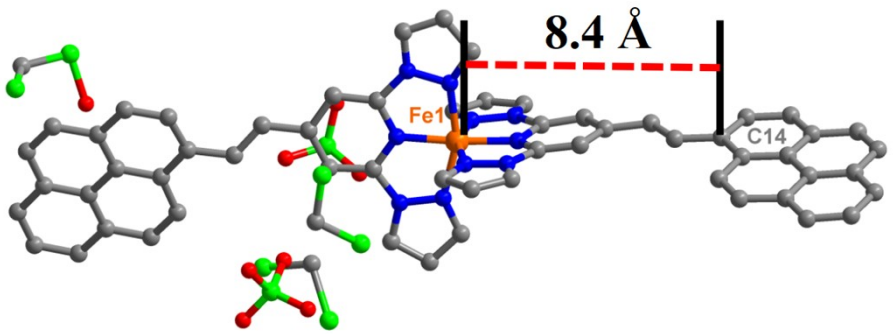

Fig. S27 Complex **2** at 120 K, the distance between the Fe^{II} center and the modified group. All H atoms and solvent molecules are omitted for clarity.

(Atomic colour scheme: Fe, orange; C, gray; O, red; N, blue; Cl, bright green).